

Achieving dynamic switchable filter based on a transmutable metasurface using SMA

Xin Chen, Jinsong Gao, and Bonan Kang

Citation: *AIP Advances* **7**, 095025 (2017); doi: 10.1063/1.5006052

View online: <https://doi.org/10.1063/1.5006052>

View Table of Contents: <http://aip.scitation.org/toc/adv/7/9>

Published by the [American Institute of Physics](#)

Articles you may be interested in

[Deposition and spin polarization study of Fe₄N thin films with \(111\) orientation](#)

AIP Advances **7**, 095001 (2017); 10.1063/1.4991963

[A visco-hyperelastic model characterizing the electromechanical behavior of nonhomogeneous soft material](#)

AIP Advances **7**, 095119 (2017); 10.1063/1.4990636

[A microfluidic approach for hemoglobin detection in whole blood](#)

AIP Advances **7**, 105102 (2017); 10.1063/1.4997185

[Competition between the inter-valley scattering and the intra-valley scattering on magnetoconductivity induced by screened Coulomb disorder in Weyl semimetals](#)

AIP Advances **7**, 105003 (2017); 10.1063/1.4998395

[Mesh parameters influence on transparent and active antennas performance at microwaves](#)

AIP Advances **7**, 085120 (2017); 10.1063/1.4985746

[Microrheology of magnetorheological silicone elastomers during curing process under the presence of magnetic field](#)

AIP Advances **7**, 095004 (2017); 10.1063/1.5002121

PHYSICS TODAY

WHITEPAPERS

MANAGER'S GUIDE

Accelerate R&D with
Multiphysics Simulation

READ NOW

PRESENTED BY

 COMSOL

Achieving dynamic switchable filter based on a transmutable metasurface using SMA

Xin Chen,^{1,2,a} Jinsong Gao,² and Bonan Kang^{1,b}

¹State Key Laboratory on Integrated Optoelectronics, College of Electronic Science and Engineering, Jilin University, Changchun 130012, China

²Key Laboratory of Optical System Advance Manufacturing Technology, Changchun Institute of Optics, Fine Mechanics and Physics, Chinese Academy of Sciences, Changchun 130033, China

(Received 23 May 2017; accepted 21 September 2017; published online 28 September 2017)

We propose a switchable filter composed of transmutable array using shape memory alloys (SMA). It could exhibit a temperature induced morphology change spontaneously like the biological excitability, acting as a shutter that allows the incident energy to be selectively transmitted or reflected with in excess of 12dB isolation at the certain frequencies for both polarizations. Equivalent circuit models describe the operational principle qualitatively and the switching effect is underpinned by the full-wave analysis. A further physical mechanism is shown by contrasting the distributions of electric field and surface current on the surface at the same frequency for the two working modes. The experimental results consist with the theoretical simulations, indicating that the metasurface could serve as one innovative solution for manipulating the electromagnetic waves and enlighten the next generation of advanced electromagnetic materials with more freedom in the processes of design and manufacturing. © 2017 Author(s). All article content, except where otherwise noted, is licensed under a Creative Commons Attribution (CC BY) license (<http://creativecommons.org/licenses/by/4.0/>). <https://doi.org/10.1063/1.5006052>

I. INTRODUCTION

Metamaterials are an engineered class of materials which exhibit properties not typically found in nature. The term metasurface has been introduced as a description for metamaterials consisting of periodic arrays of scatterers or apertures which form a surface much thinner than the design wavelength,^{1–7} such as frequency selective surface (FSS) which is recognized as the foundation of the field of metamaterials has been widely used in the microwave and optical domains for decades due to its functionality of spectral selectivity.^{8–12} Compared with the conventional FSS, the frequency response of a switchable filter can be varied with time under the control of active devices incorporated into the unit cells, such as PIN diodes^{13–16} and microelectromechanical systems (MEMS) switches,^{17,18} or by utilizing a ferrite,¹⁹ liquid crystal²⁰ or elastomer²¹ as the substrate. However, all the attempts exhibit unavoidable drawbacks including insertion losses, pass-band fluctuations, unwanted resonances, high cost, complexity of the fabrication and lack of the design flexibility. Another kind of method is the use of structurally reconfigurable metamaterials,^{22–24} but the previous works are operated under extreme temperatures and the modulation depths are not good enough. So there exist great demands for a superior performance and high efficient switchable spatial filter.

In the natural world, many animals display dramatic change of hue and brightness derived from astonishingly intricate three-dimensional biomaterials whose morphologies could vary naturally with a proper stimulation from the outer environment.^{25–28} Inspired by the changeable structure color and

^achenxin.19344834@163.com

^bkangbn@jlu.edu.cn

the excitability of living organism, we design and fabricate a contrasting class of switchable spatial filter based on a transmutable metasurface using SMA. The meta-cell could convert its morphology from one geometrical shape to the other spontaneously during the variation of ambient temperature just as the organism responds to the external stimulation, which enables the metasurface to be either transmissive or reflective at the frequencies of interest, setting us free from the bondages of active devices and diverse substrates. We use the equivalent circuit models to predict the electromagnetic behavior of the surface and the switchable capability is demonstrated by full-wave analysis. A satisfactory agreement between the experimental and numerical transmission curves is obtained, and the part of discussion could serve as a basic study for the effect of array restructure on a reconfigurable metasurface. Furthermore, the highly controllable mechanism of engineering and manipulating the transmission characteristic of the transmutable metasurface will be a valuable reference for the application in engineering development.

II. MODEL DESIGN AND ANALYSIS

For ensuring the transmission characteristic of the surface to be identified easily and processing conveniently, we choose the derivatives of circular loop aperture element as the unit cells and propose the design concept by introducing the equivalent circuit models which enable us to synthesize the transmutable array from system level performance indicators without having to analyze in detail the behavior of each unit cell in combination with its neighbors.

When the unit cell consists of a circular aperture element as shown in Fig. 1(a), the surface can be deemed as composed of infinitely long bars in the vertical direction leading to the inductance L_1 across an equivalent transmission line for TE polarization. The horizontal bars will act like capacitors primarily in parallel with the inductors and will not generate horizontal inductances. However, Fig. 1(a) shows an inductive element because the equivalent capacitance C_0 is too small to produce a valid resonance with high quality factor of the parallel circuit. If we put a disk inside the aperture as shown in Fig. 1(b), the unit cell becomes a circular loop aperture element which owns the large capacitance C_1 and raises the quality factor of the parallel resonant circuit. The transmission characteristics of the two elements will not change for TM polarization due to the symmetry of their structures. When the disk connects to the right edge of the aperture with a strip, its shape becomes similar to the biological tentacle and the equivalent circuit model can be thought of as two different transmission line circuits corresponding to TE and TM polarization respectively as shown in Fig. 1(c) and Fig. 1(d). For TE polarization the equivalent circuit model is the same to Fig. 1(b), but for TM polarization the strip converts the region of existing capacitance C_1 to approximate inductance L_2 and out of the connection still remain capacitors with smaller capacitance C_2 . The surface impedance in Fig. 1(d) is following the Eq. (1) that provides two resonant frequencies contrary to the case of TE polarization with one pole of the Eq. (2), the lower resonant frequency is mostly determined by L_1 and C_1 which own the larger values, whereas the higher resonant frequency mainly depends on the smaller inductance L_2 and capacitance C_2 . Because of the huge differences between C_1 and C_2 , L_1 and L_2 , the two resonant frequencies are separated by great distance in the transmission spectrum, so we have to consider the onset of grating lobes for TM polarization. The frequency f_g where a grating lobe is encountered under normal incidence is determined by Eq. (3),⁹ the grating lobe indexes (k, n) which satisfy the Eq. (3) are those values different from (0,0), D_x and D_y denote the element spacing

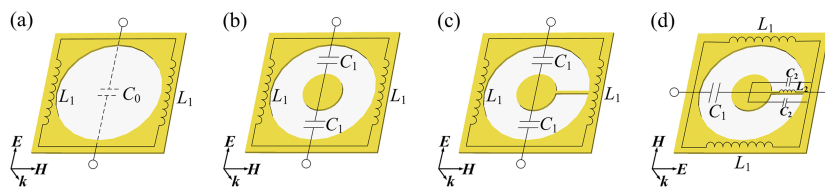


FIG. 1. Equivalent circuit model for TE polarization of (a) circular aperture element, (b) circular loop aperture element, (c) shorted circular loop aperture element and for TM polarization of (d) shorted circular loop aperture element.

in the X direction and Y direction respectively.

$$Z_{TM} = \frac{-2j\omega^3 L_1 L_2 C_2 - j\omega^3 L_1 L_2 C_1 + j\omega L_1}{2\omega^4 L_1 L_2 C_1 C_2 - 4\omega^2 L_2 C_2 - 2\omega^2 L_2 C_1 - \omega^2 L_1 C_1 + 2}, \quad (1)$$

$$Z_{TE} = \frac{2j\omega L_1}{4 - \omega^2 L_1 C_1}, \quad (2)$$

$$\left(k \frac{c}{f_g \cdot D_x}\right)^2 + \left(n \frac{c}{f_g \cdot D_y}\right)^2 = 1. \quad (3)$$

Qualitative analysis from the equivalent circuit models imply that we could modify the transmission characteristic of the surface by switching the morphology of the unit cell between two different geometrical shapes corresponding to the transmissive mode and the reflective mode respectively as depicted in Fig. 2: if the tentacle stretches out of the aperture for TE polarization, the morphology of the unit cell will convert from the transmissive structure of resonant element to the reflective structure of approximately inductive element, which leads to a great change in transmission characteristic of the surface; when switching in the same way for TM polarization, it will have a huge influence on the lower resonant frequency because the large distance bring about a small capacitance paralleled with the horizontal bars as previously mentioned, meanwhile the values of C_2 and L_2 will also change due to the variation of spatial relationship between the tentacle and the vertical bar on the right side, which results in the drift of the higher resonant frequency accordingly. What is said above indicates the operational principle of the workable model.

For getting a vivid illustration of the behavior of the equivalent circuit models, full-wave analysis of the metasurface is performed. A three-dimensional view of the unit cell structure is shown in Fig. 3(a) including the design parameters. Fig. 3(b) shows that the transmission characteristic of the metasurface highly depends on the morphology of the unit cell under normal incidence for both polarizations, demonstrating the consequences predicted by the equivalent circuit models. When the tentacle stays in the aperture of the surface and $\alpha=180^\circ$ for TE polarization, the unit cell becomes a resonant structure composed of the shorted circular loop aperture element that could transmit the energy impinging on it at 23.3GHz and exhibit a small transmission loss of less than 0.3dB;

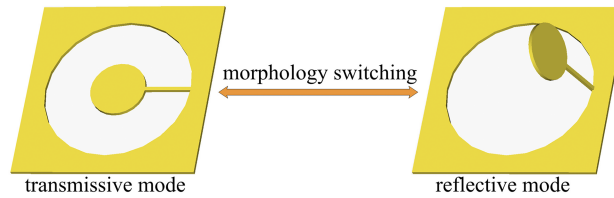


FIG. 2. Operational principle of the model: morphology switching between two different elements.

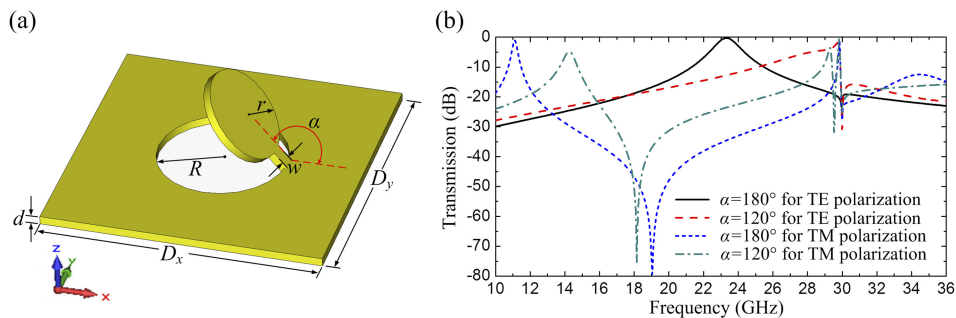


FIG. 3. (a) 3D schematic of the unit cell, where $D_x=D_y=10\text{mm}$, $d=0.3\text{mm}$, $w=0.5\text{mm}$, $R=2.3\text{mm}$ and $r=2.1\text{mm}$, the impinging plane wave propagates along Z direction. (b) Frequency response obtained from full-wave simulation with different values of α for both polarizations.

when the tentacle stretches out of the aperture and $\alpha=120^\circ$, we obtain an embossed reflector with a good isolation of more than 12dB from transmissive mode at the original resonant frequency, certifying the signal rejection in the mentioned frequency band. For TM polarization we verify that the surface has the ability of switching at 11.1GHz but suffers a failure at 30GHz where we see the grating lobe as predicted by Eq. (3) no matter what the value of α is. Thus take no account of the invalid dual-band switchable filter, we develop a new type of freestanding switchable band-pass filter using a thin self-supporting and air-spaced metasurface composed of the transmutable array, in which the transmittance can be switched at 23.3GHz for TE polarization and at 11.1GHz for TM polarization.

III. FABRICATION AND EXPERIMENTAL VERIFICATION

An experimental verification should be accomplished to show the effectiveness and feasibility of the described model. The selection of fabrication material is implemented as the first step of the manufacture and the ideal material for the metasurface should contain the following features: high conductivity, transforming the shape spontaneously with external stimulation and compatibility with existing fabrication processes. The material chosen to meet these requirements is SMA with the two way shape memory effect (TWSME). It refers to the reversible and spontaneous shape change of materials which could exhibit a geometrical shape at high temperature phase (austenite) and another shape at low temperature phase (martensite).²⁹ This uncommon behavior is not intrinsic to SMA but an induced phenomenon through thermal treatment and training, and what is involved in both kinds of phenomena is either transformation between martensite and austenite.³⁰

The specimen of 300mm×300mm×0.3mm in dimension is spark cut from the plate of single crystal after hot-rolled and cold-rolled with a nominal composition of copper(69.61wt.%), zinc (25.7wt.%), aluminum(3.81wt.%), nickel(0.8wt.%), lanthanum(0.04wt.%) and cerium(0.04wt.%), the aforementioned shorted circular loop aperture element is realized by machining operation.^{31–33} Thermal treatment could be described as follows: the specimen is heated at 850°C for 30min in vacuum followed by oil quenching at 25°C rapidly, afterwards quenched into the silicon oil at 150°C for 30min, and finally quenched into the water at 50°C for 15min.³¹ Thus we find the values of characteristic temperatures at stress free state: $M_s=64^\circ\text{C}$, $M_f=52^\circ\text{C}$, $A_s=58^\circ\text{C}$, $A_f=70^\circ\text{C}$. M_s , M_f , A_s and A_f represent martensitic transformation start and finish temperature and austenite transformation start and finish temperature respectively, the temperature hysteresis $\Delta T=A_f - M_s=6^\circ\text{C}$.

The specimen is trained in bending the tentacles according to the procedure known as “thermal training under constrain”.^{34–36} Firstly, heating the surface higher than 70°C to the high temperature phase with electric heaters then bend the tentacle of each unit cell out of the aperture slowly to the deformation position where the value of α is about 110°; secondly, sustain the morphology with stress as cooling it to room temperature; thirdly, unload the stress and the tentacles will spring back slightly; at last reheating the surface to the high temperature phase and the tentacles continue to move spontaneously in the same direction until the value of α is about 170° for shape recovery. Repeat the above steps 8 times.

By this means the transmutable metasurface achieves a reversible and macroscopic shape change depending on temperature without any additional mechanical loading, as the living organism responses to the stimulation of ambient environment: when the specimen is heated over 58°C, the meta-cells start to draw back their tentacles and recover to the heating morphology until the temperature is higher than 70°C, then the value of α is about 170° that we could put a clip on the tentacles easily as shown in Fig. 4(a), the whole process takes less than five seconds and the response time highly depends on the distance between the electric heaters and the specimen; after the temperature of the specimen drops below 64°C, the meta-cells set about stretching out their tentacles to push away the clip corresponding to the cooling morphology and at last the value of α is about 120° at room temperature as shown in Fig. 4(b).

As shown in Fig. 5, the measurement is carried out in a microwave anechoic chamber using two horn antennas connected by a vector network analyzer, a microwave absorber on every side of the specimen is set to minimize the measurement errors, two electric heaters are used for heating the specimen to assure the temperature is high enough. Fig. 6(a) shows the marvelous ability of

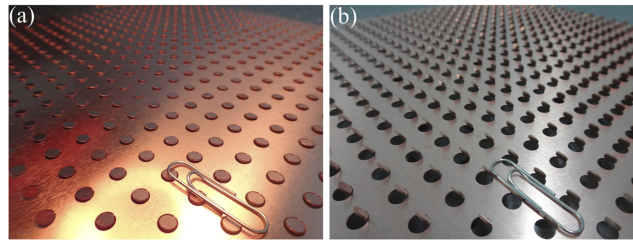


FIG. 4. The morphologies of the metasurface with external stimulation of (a) high temperature and (b) low temperature.

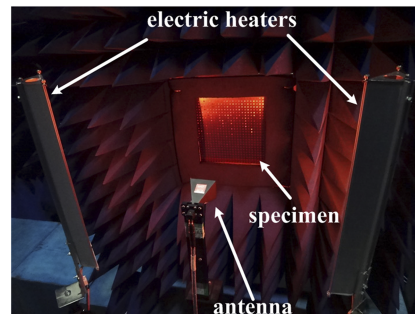


FIG. 5. The experimental setup for measurement in the microwave chamber, which includes a couple of antennas, two electric heaters and the tested metasurface.

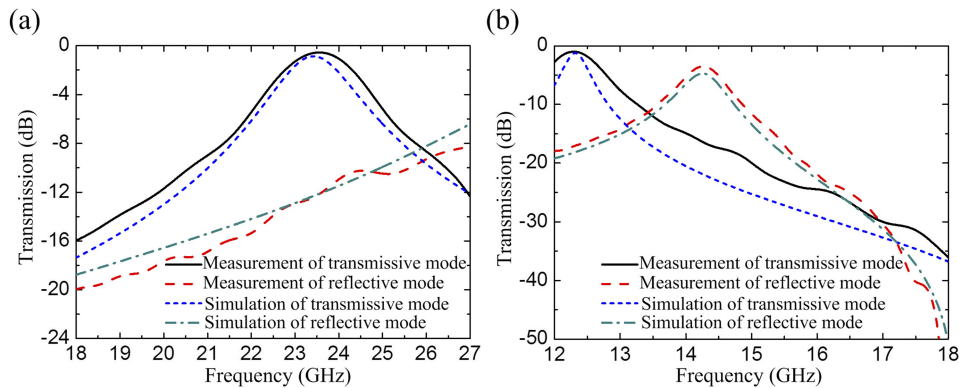


FIG. 6. Comparison between measurement and simulation for two working modes under (a) TE polarization and (b) TM polarization.

switching for TE polarization: when heating the specimen to the high temperature phase we find that the pass-band is centered at 23.5GHz with a small insertion loss of 0.47dB; if we stop heating and the temperature of the specimen drops down enough, more than 12dB attenuation will be observed at the original resonance frequency. For TM polarization the peak value is -0.99dB at 12.3GHz and we get an even better isolation of 15.5dB between two working modes as shown in Fig. 6(b). The curve trends of measurements and simulations are similar with each other for the same working mode, some slight frequency deviations may be ascribed to the manufacturing tolerance of the unit cell and the disparity of bending angle of the tentacles produced in the training process. Besides, the dimension of the specimen is fixed while being set as infinite periodic structure in simulation. However, this experiment confirms the reliable and efficient performance of the metasurface.

IV. DISCUSSION

To better understand the impact of morphology switching of the unit cell on the transmission characteristic, we can gain some insight into the variations of the electric field strength and surface current distribution on the surface at resonance frequency as shown in Fig. 7 and Fig. 8 when the value of α is different for both polarizations. The color map indicates the gradient electric field distributions and the arrows represent the directions of the surface currents during half cycle.

For TE polarization, at 23.3GHz there are strong electric fields distributing on the edges of the gaps at the top and bottom of the aperture when the tentacle stays in the aperture as shown in Fig. 7(a), that is because the maximal surface current is induced around the two flanks of the shorted circular loop aperture and flows along the edges of inner disk and outer bars in the opposite directions as show in Fig. 7(c), which results in the conspicuous charge accumulation in the capacitors derived from the gaps aforementioned. It predicts that there will be significant changes in the electric field distribution and the transmission spectrum if we can modify the distribution of surface current on the patterned surface. Then, by morphology switching the surface current declines significantly along the flow direction as shown in Fig. 7(d) at the same frequency, the reduction of the surface current weakens the charge accumulation and thus the electric field strength as shown in Fig. 7(b) as anticipated, and another profound consequence is that the variation of surface current distribution on the surface destroys the original resonance, leading to an obvious descent of the transmittance at the initial resonant frequency when the value of α is 120° . That means the peak of the transmission spectrum is corresponding to the emergence of the maximal surface current on the surface, hence we can manipulate the transmission characteristic of the metasurface by transforming the morphology of the unit cell and then altering the surface current distribution on the metal structure.

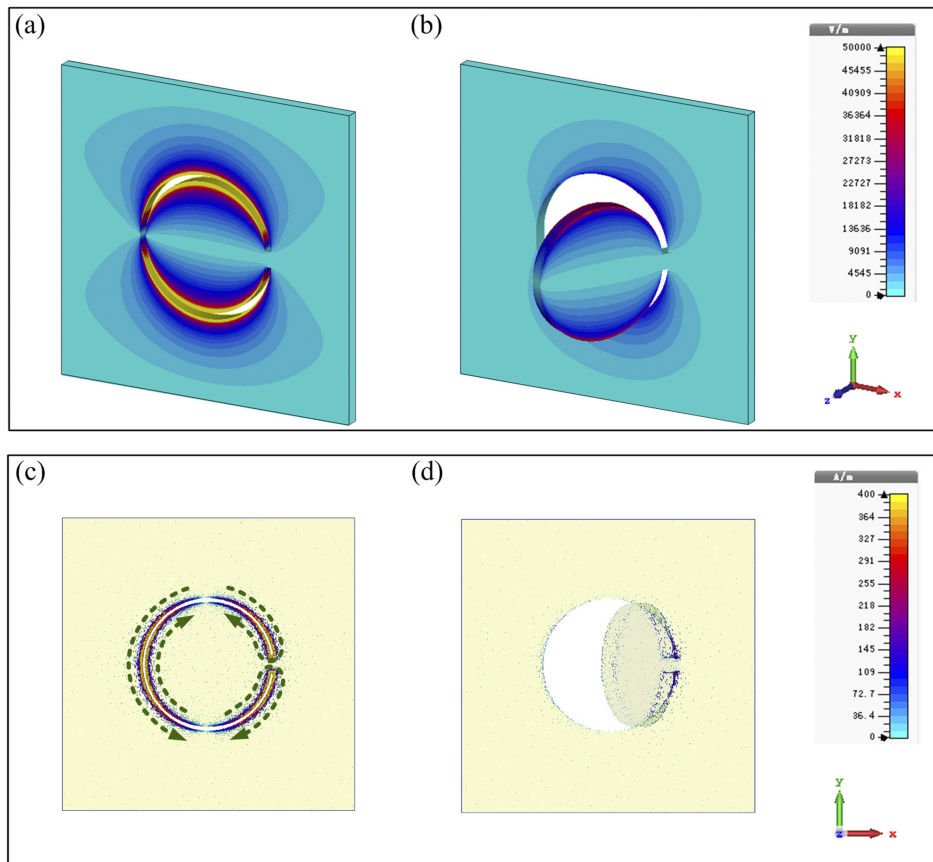


FIG. 7. Distributions of the electric fields (a, b) and surface currents (c, d) for TE polarization under normal incidence when $\alpha=180^\circ$ (a, c) and $\alpha=120^\circ$ (b, d) at 23.5GHz.

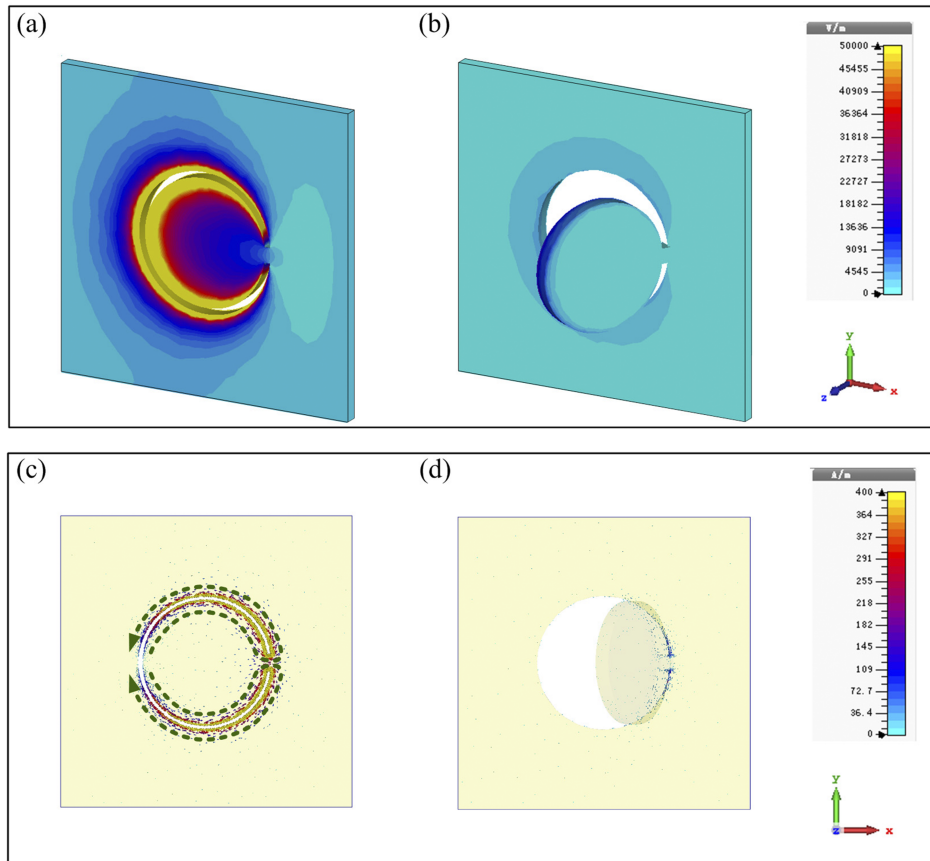


FIG. 8. Distributions of the electric fields (a, b) and surface currents (c, d) for TM polarization under normal incidence when $\alpha=180^\circ$ (a, c) and $\alpha=120^\circ$ (b, d) at 11.1GHz.

For TM polarization, the change rules of the electric field strength and surface current distribution on the surface at 11.1GHz are similar to that of TE polarization when the value of α is different as shown in Fig. 8. From the above descriptions we get a deeper understanding of the switching mechanism of the transmutable metasurface.

V. CONCLUSION

Here, we report on the design, fabrication and measurement of a dynamic switchable spatial filter based on a transmutable metasurface with significant improvements in performance and design flexibility. The metallic tentacles of the metasurface could stretch out as well as shrink back in accordance with our expectation by applying a suitable variation range of ambient temperature, which results in the changes of the surface current distribution on the metal structure and the transmittance of the surface. Numerical data, both from simulations and measurements, are presented to validate that the switchable attenuation of more than 12dB will occur at disparate frequencies for different polarizations when the two different morphologies of the meta-cell convert to each other alternately. This paper presents a flexible paradigm for manipulating the spectral response of switchable metasurface without using any form of active devices or substrates, opening up new design concept for realizing high efficient reconfigurable metasurface over an ultra-wide frequency range.

ACKNOWLEDGMENTS

This work is supported by the National Natural Science Foundation of China (NSFC) (61401424).

- ¹ C. L. Holloway, E. F. Kuester, J. A. Gordon, J. O'Hara, J. Booth, and D. R. Smith, *IEEE Antennas Propag. Mag.* **54**, 10 (2012).
- ² Q. Feng, M. Pu, C. Hu, and X. Luo, *Opt. Lett.* **37**, 2133 (2012).
- ³ P. E. Sieber and D. H. Werner, *Opt. Express* **21**, 1087 (2013).
- ⁴ C. Argyropoulos, K. Q. Le, N. Mattiucci, G. D'Aguanno, and A. Alù, *Phys. Rev. B* **87**, 205112 (2013).
- ⁵ S. Maci, G. Minatti, M. Casaletti, and M. Bosiljevac, *IEEE Antennas Wirel. Propag. Lett.* **10**, 1499 (2011).
- ⁶ J. D'Archangel, E. Tucker, E. Kinzel, E. A. Muller, H. A. Bechtel, M. C. Martin, M. B. Raschke, and G. Boreman, *Opt. Express* **21**, 17150 (2013).
- ⁷ S. Walia, C. M. Shah, P. Gutruf, H. Nili, D. R. Chowdhury, W. Withayachumnankul, M. Bhaskaran, and S. Sriram, *App. Phys. Rev.* **2**, 011303 (2015).
- ⁸ N. I. Zheludev, *Science* **328**, 582 (2010).
- ⁹ B. A. Munk, *Frequency Selective Surfaces: theory and Design* (John Wiley and Sons, 2000).
- ¹⁰ B. Li and Z. X. Shen, *Appl. Phys. Lett.* **103**, 171607 (2013).
- ¹¹ J. D'Archangel, E. Tucker, M. B. Raschke, and G. Boreman, *Opt. Express* **22**, 16645 (2014).
- ¹² T. K. Wu, *Frequency Selective Surface and Grid Array* (John Wiley and Sons, 1995).
- ¹³ H. Fabian-Gongora, A. E. Martynyuk, J. Rodriguez-Cuevas, and J. I. Martinez-Lopez, *IEEE Microw. Wireless Compon. Lett.* **25**, 606 (2015).
- ¹⁴ G. I. Kiani, K. L. Ford, L. G. Olsson, K. P. Esselle, and C. J. Panagamuwa, *IEEE Trans. Antennas Propag* **58**, 581 (2010).
- ¹⁵ B. Sanz-Izquierdo, E. A. Parker, and J. C. Batchelor, *IEEE Trans. Antennas Propag.* **59**, 2728 (2011).
- ¹⁶ B. Sanz-Izquierdo, E. A. Parker, and J. C. Batchelor, *IEEE Trans. Antennas Propag.* **58**, 3761 (2010).
- ¹⁷ B. Schoenlinner, A. Abbaspour-Tamijani, L. C. Kempel, and G. M. Rebeiz, *IEEE Trans. Microw. Theory Tech.* **52**, 2474 (2004).
- ¹⁸ F. Ma, Y. S. Lin, X. Zhang, and C. Lee, *Light-Sci. Appl.* **3**, e171 (2014).
- ¹⁹ E. A. Parker and S. B. Savia, *IEE Proc. -Microw. Antennas Propag.* **148**, 103 (2001).
- ²⁰ W. Hu, R. Dickie, R. Cahill, H. Gamble, Y. Ismail, V. Fusco, D. Linton, N. Grant, and S. Rea, *IEEE Microw. Wireless Compon. Lett.* **17**, 667 (2007).
- ²¹ I. M. Pryce, K. Aydin, Y. A. Kelaita, R. M. Briggs, and H. A. Atwater, *Nano Letter* **10**, 4222 (2010).
- ²² H. Tao, A. C. Strikwerda, K. Fan, W. J. Padilla, X. Zhang, and R. D. Averitt, *Phys. Rev. Lett.* **103**, 147401 (2009).
- ²³ J. Y. Ou, E. Plum, L. Jiang, and N. I. Zheludev, *Nano Letter* **11**, 4222 (2010).
- ²⁴ A. Karvounis, J. Y. Ou, W. Wu, K. F. MacDonald, and N. I. Zheludev, *Appl. Phys. Lett.* **107**, 191110 (2015).
- ²⁵ S. V. Saenko, J. Teyssier, D. Marel, and M. C. Milinkovitch, *BMC Biol.* **11**, 105 (2015).
- ²⁶ D. Gur, B. A. Palmer, S. Weiner, and L. Addadi, *Adv. Funct. Mater.* **27**, 1603514 (2017).
- ²⁷ J. Teyssier, S. V. Saenko, D. Marel, and M. C. Milinkovitch, *Nat. Commun.* **6**, 6368 (2015).
- ²⁸ D. Gur, B. A. Palmer, B. Leshem, D. Oron, P. Fratzl, S. Weiner, and L. Addadi, *Angew. Chem. Int. Ed.* **54**, 12426 (2015).
- ²⁹ A. Amengual, E. Cesari, and R. Romero, *Scr. Metall. Mater.* **32**, 1269 (1995).
- ³⁰ E. Cingolani, M. Ahlers, and M. Sade, *Acta Metall. Mater.* **43**, 2451 (1995).
- ³¹ G. F. Xu, *Res. Stud. Foundry Equip.* **23**, 20 (2001).
- ³² G. F. Xu, N. C. Si, and Y. X. Li, *Chin. J. Nonferrous Met.* **14**, 825 (2004).
- ³³ Y. Bellouard, *Proceedings of the 7th European Symposium on Martensitic Transformations* (Elsevier, 2008), pp. 582.
- ³⁴ Y. Liu, Y. Liu, and J. V. Humbeeck, *Acta Mater.* **47**, 199 (1998).
- ³⁵ X. L. Meng, Y. F. Zheng, W. Cai, and L. C. Zhao, *J. Alloys Compd.* **372**, 180 (2004).
- ³⁶ D. A. Miller and D. C. Lagoudas, *Mater. Sci. Eng. A* **308**, 161 (2001).